Inorganic Chemistry

pubs.acs.org/IC Article

Synthesis and Growth of Rare Earth Borates $NaSrR(BO_3)_2$ (R = Ho–Lu, Y, Sc)

Artem B. Kuznetsov,* Konstantin A. Kokh, Nursultan Sagatov, Pavel N. Gavryushkin, Maksim S. Molokeev, Valery A. Svetlichnyi, Ivan N. Lapin, Nadezda G. Kononova, Vyacheslav S. Shevchenko, Asset Bolatov, Bolat Uralbekov, Anastasia A. Goreiavcheva, and Alexander E. Kokh

Cite This: *Inorg. Chem.* 2022, 61, 7497–7505 Read Online

ACCESS | Metrics & More | Article Recommendations | Supporting Information

ABSTRACT: $NaSrR(BO_3)_2$ (R = Ho–Lu, Y, Sc) compounds were obtained for the first time. Their structures exhibit disordered positions of Sr^{2+} and Na^+ atoms while RO_6 polyhedra are connected through the BO_3 groups. Large distances between R atoms and high transparency in the range of 250–900 nm make them promising for phosphor applications. A pathway to obtain single crystals was shown by growing $NaSrY(BO_3)_2$ and $NaSrYb(BO_3)_2$ by the top seeded solution growth method with Na_2O-B_2O_3-NaF flux.

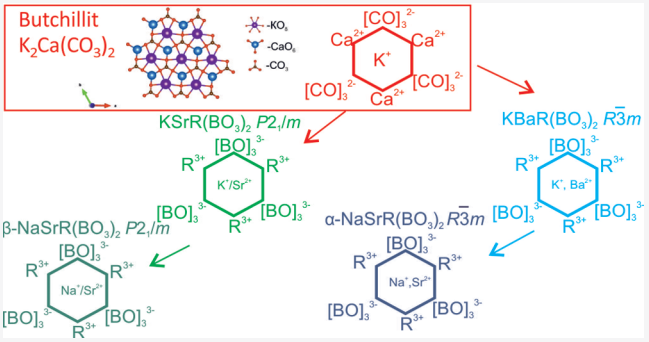

INTRODUCTION

Today, a large portion of the scientific community is aimed to obtain environmentally friendly light sources and phosphors with applications in the near-infrared range (800–820 and 900–980 nm).[1−6] Borates are among the promising candidates due to their high chemical, thermal, and radiation stabilities and wide transparency range. Recent discoveries of alkaline and/or alkaline earth borates have resulted in use of higher concentrations of rare earth elements to achieve high luminescence efficiency.[7−11]

New $NaBaSc(BO_3)_2$ and $NaBaY(BO_3)_2$ compounds were obtained by means of (Ba^{2+}/Na^+) replacement in $Na_3R(BO_3)_2$ and $Ba_3R(BO_3)_3$.[12,13] It was established that $NaBaR(BO_3)_2$, R = Sc, Y have order–disorder polymorphic transitions at 775 ± 20 °C and 375 ± 30 °C, respectively. New high-temperature polymorphic modifications are solid solutions based on $(Ba,Na)_2R(BO_3)_2$, R = Sc, Y, which are characterized by a disordered distribution of Ba and Na atoms and a halved *c* axis.

The discovery of three cationic borates initiated a large number of works on their doping with REE atoms[14−17] and opened a tremendous field of isomorphic substitutions in the positions of 1+, 2+, and 3+ ions for various combinations. Thus, in subsequent works, the following compounds $KBaR(BO_3)_2$,[18,19] $KCaR(BO_3)_2$,[20] $Li_3Ba_4Sc_3B_8O_{22}$,[21] $LiBaTb_2(BO_3)_3$,[22] $KSrY(BO_3)_2$,[23] $NaSr_4La_3(BO_3)_6$,[24] and $K_7MIIIRE_2(B_5O_{10})_3$[25−27] were discovered. Another motivation for this study is the fact that borates containing sodium are one of the most popular phosphors.[28−33] For example, $Na_3R(BO_3)_2$ (R = Y, La, Nd, Gd) crystallizing in the $R\bar{3}$ space group has a low concentration quenching of luminescence.[31−33]

In the present investigation, we report the synthesis, growth of the bulk crystals, and luminescent properties of $NaSrR(BO_3)_2$ compounds. A discussion of the two crystal structures' thermal and optical properties is given.

EXPERIMENTAL SECTION

Powdered samples of $NaSrR(BO_3)_2$ (R = Ho–Lu, Y, Sc) were prepared by the method of the two-stage solid-state synthesis in a Pt crucible. In the first stage, stoichiometric mixtures of pure raw Na_2CO_3, $SrCO_3$, H_3BO_3 and R_2O_3 reactants in molar ratios of 1:2:4:1 were heated at 650 °C for 5 h to decompose Na_2CO_3, $SrCO_3$, and H_3BO_3. In the second stage, the mixtures were ground in an agate mortar, pressed into pellets, and heated again at 900 °C for 12 h until the complete disappearance of initial reagents, checked by powder XRD.

The scheme of the solid-state reaction can be suggested as follows:

$$Na_2CO_3 + 2SrCO_3 + R_2O_3 + 4H_3BO_3 = 2NaSrR(BO_3)_2 + 6H_2O + 3CO_2$$

Received: February 21, 2022
Published: May 3, 2022

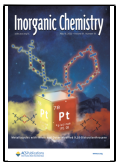

Downloaded via STATE PUBLIC SCITECH LIBRARY SB RAS on July 12, 2022 at 05:22:08 (UTC).
See https://pubs.acs.org/sharingguidelines for options on how to legitimately share published articles.

ACS Publications © 2022 American Chemical Society

https://doi.org/10.1021/acs.inorgchem.2c00596
Inorg. Chem. 2022, 61, 7497–7505

Using Na_2O-B_2O_3-NaF flux,[34] $NaSrR(BO_3)_2$ (R = Y, Yb) crystals with a transparent area of 5 × 5 × 5 mm^3 were grown. A charge for the growth experiment comprised of presynthesized $NaSrR(BO_3)_2$ (R = Y, Yb) and Na_2CO_3, H_3BO_3, NaF in a molar ratio of 3:5:5:6. A Pt crucible with the charge was heated to 700 °C and held a day to achieve melt homogenization. Then, the temperature was decreased at the rate of 2 °C day^{-1} from 700 °C to 600 °C. After that, the furnace was cooled to room temperature at the rate of 15 °C day^{-1}.

Powder X-ray diffraction patterns of the $NaSrR(BO_3)_2$ (R = Ho−Lu, Y, and Sc) powdered samples were obtained with the XRD 7000 (Shimadzu, Japan) diffractometer in Bragg−Brentano geometry using Cu Kα radiation at room temperature (Figure S1) and at 600 °C with heat chamber equipment (Figure S2). The crystal structure of β-$NaSrY(BO_3)_2$ was refined by thr Rietveld method which was performed using TOPAS 4.2.[35] The crystal structure of $KSrY(BO_3)_2$[23] was used as the starting model for refinements with K^+ replaced by Na^+ ion. All ions were refined with isotropical thermal parameters; moreover all O^{2-} ions were refined with one thermal parameter in order to reduce the number of parameters. There are two sites occupied both by Sr and Na atoms in the asymmetric part of the unit cell and both of them were occupied by Sr/Na ions in our model. The p(Na) and p(Sr) occupancies were refined within linear restriction p(Sr) + p(Na) = 1 for each site. Final refinements were stable and gave low *R*-factors. Summary data about the XRD, data-collection parameters, the structure refinement, and difference Rietveld plot of $NaSrY(BO_3)_2$ are listed in Table S1 and Figure S3, whereas final atomic coordinates and equivalent isotropic displacement parameters are reported in Table S2. In addition, lattice parameters of α- and β-$NaSrR(BO_3)_2$ were obtained by the LeBail method[36,37] within the GSAS-II program (Tables S3 and S4).

The chemical composition of the obtained crystals (Na-Sr-R relationships) was approved by X-ray fluorescent analysis using an XRF 1800 (Shimadzu, Japan).

The DSC (differential scanning calorimetry) curves of the $NaSrR(BO_3)_2$ crystals were measured with the scanning thermal analyzer 449 F5 Jupiter (Netzsch, Germany) in shared research facilities for multielemental and isotope studies of the SB RAS. In total, 50 mg of powdered $NaSrR(BO_3)_2$ sample was heated in a platinum crucible with argon as a shield gas from room temperature to 1300 °C at the rate of 10 K min^{-1}. An empty Pt crucible was used as the standard.

Diffuse reflectance spectra of $NaSrR(BO_3)_2$ powders were recorded at room temperature using a Cary 100 (Varian, Australia) spectrophotometer with a diffuse reflectance accessory DRA-CA-30I (Labsphere, USA) in the range of 200−900 nm and by a FTIR spectrometer Nicolet 6700 (Thermo Fisher Scientific, USA) in the range of 11000−400 cm^{-1}. The optical band gap width was estimated by the Tauc[38] method for a nonstraight-band semiconductor. Also the absorption spectrum differentiation (DASF) method was used, which does not require taking into account the type of optical transitions.[39]

Raman spectra were collected by using a confocal Raman microscope InVia (Renishaw, U.K.) with a spectral resolution of 1 cm^{-1} equipped with a Leica optical microscope (with a 50× objective) and a Peltier cooled Si detector, under 100 mW CW Nd:YAG laser excitation, operating at 532 nm, in the range of 100−3200 cm^{-1}.

High-resolution luminescence spectra of powdered $NaSrR(BO_3)_2$ were collected using the same InVia Raman microscope under the excitation with a 532 nm at 5% power and 50% defocus in the range of 540−1060 nm.

All calculations have been performed within the density functional theory (DFT) implemented in the VASP package.[40,41] The exchange−correlation interaction was taken into account in the generalized gradient approximation in the form of the Perdew−Burke−Ernzerhof scheme.[42] The optimization parameters were as follows: the cutoff energy of the plane wave basis −1000 eV, the electronic smearing, according to the Gaussian scheme, σ = 0.05 eV, and k-point grid −4 × 6 × 6 for the low-temperature phase and 6 × 6 × 3 for the high-temperature phase. Densities of states (DOS) were calculated using 10 × 14 × 14 and 15 × 15 × 9 grids of k-points for the low-temperature and high-temperature phases, respectively. Also to obtain more accurate band gaps of $NaSrY(BO_3)_2$-$P2_1/m$, the HSE06 hybrid functional[43−45] was used.

To calculate the IR spectra, the density functional perturbation theory implemented in VASP was used. In order to obtain the Raman spectra, the polarizability tensors for each crystal mode were calculated using the *vasp_raman.py* code.[46]

To examine the dynamic stability of low-temperature and high-temperature phases of $NaSrY(BO_3)_2$, molecular dynamic (MD) simulations were performed. The MD simulations were carried out in the isothermal−isobaric *NPT* ensemble (*N*, the number of particles; *P*, pressure; and *T*, temperature). The Langevin thermostat was used to control the frequency of the temperature oscillations during the simulations. The time step was set to 1 fs, and the total simulation time was 10 ps. The low-temperature phase was approximated by the supercells containing 264 atoms, which are a 2 × 3 × 2 supercell of the unit cell used. For the high-temperature phase, an orthohexagonal cell with 264 atoms was used.

RESULTS AND DISCUSSION

XRD patterns of $NaSrR(BO_3)_2$ (R = Ho−Lu, Y, Sc) recorded at room temperature are shown in Figure S1. The absence of impurities of the initial components was achieved at the synthesis temperature of 850−900 °C, which is in good agreement with the work for similar compounds.[7,16,19,22,47]

Figure 1 presents DSC curves for $NaSrR(BO_3)_2$ (R = Ho−Lu, Y, Sc) compounds. There is an intense endothermic peak in the temperature range of 1054.8 °C (Ho)−1206 °C (Lu) corresponding to the melting phenomenon. The compounds with Y and Ho melt incongruently, while other (Er−Lu) are congruent. Also, all compounds have a minor endothermic peak in the temperature range of 457.7 °C (Y)−548.4 °C (Lu) assumed to be the phase transition. To confirm that, *in situ* measurements of the XRD patterns at 600 °C for $NaSrR(BO_3)_2$ (R = Ho, Er, Yb, and Y) were performed (Figure S2). Both phase transition and melting temperatures have a pronounced dependence on the rare earth radius. For example, the compounds with larger Y and Ho have a lower temperature than those with Lu and Sc (Figure 1c).

Figure 2a,b shows $NaSrR(BO_3)_2$ (R = Yb and Y) crystals grown from the Na_2O-B_2O_3-NaF flux at ∼700 °C. The single crystal plates up to 10 mm^2 without visible inclusions were selected (Figure 2c,d); however, the examination in polarized light has shown multiple boundaries of polysynthetic twinning (Figure 2e,f), which make the crystals unsuitable for further study by optical methods. Based on the concentric distribution of the twin boundaries, we assume them to be produced during the cooling of the crystals.

Figure 3 presents XRD patterns of different $NaSrY(BO_3)_2$ samples. It can be concluded that grown crystals and synthesized samples have the same diffraction pattern, while *in situ* measurements at the temperature above the phase transition resulted in some rearrangement of the peaks. Comparison of the obtained patterns with those of related three-cation compounds showed their principal similarity with $KBaY(BO_3)_2$ and $KSrY(BO_3)_2$ for high-temperature α- and low-temperature β-modifications, correspondingly. The same behavior was found for all $NaSrR(BO_3)_2$ samples. It was impossible both to quench the high-temperature modification and to perform direct crystallization of the low-temperature phase from the flux. Therefore, a further study of the crystals obtained only by the solid-phase synthesis was carried out.

From powder XRD it is clearly seen (Figure S1) that all $NaSrR(BO_3)_2$ samples are isostructural. We describe their

https://doi.org/10.1021/acs.inorgchem.2c00596
Inorg. Chem. 2022, 61, 7497−7505

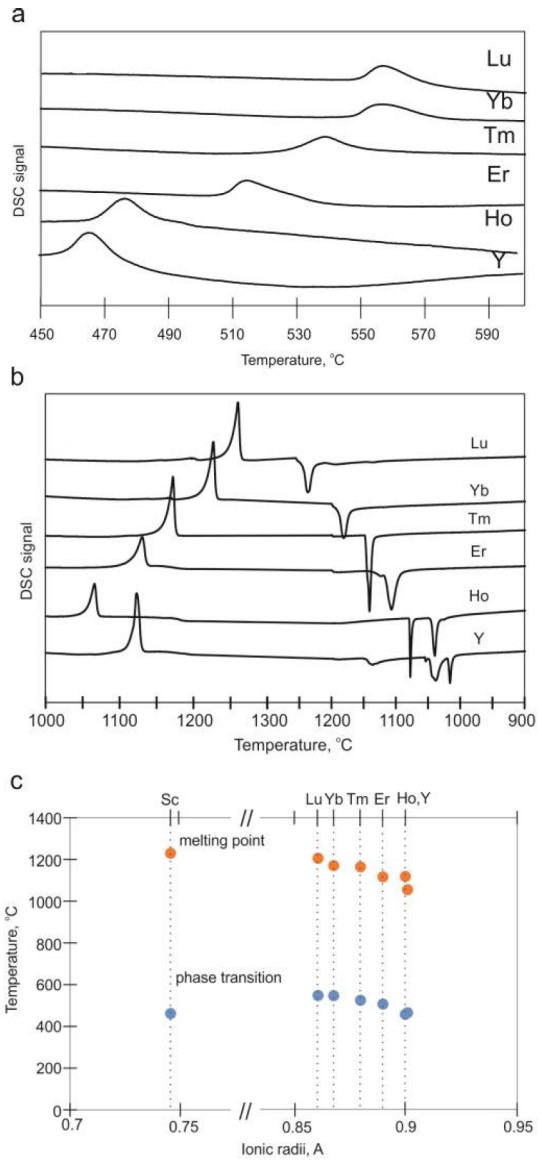

Figure 1. DSC curves of $NaSrR(BO_3)_2$ (R = Ho−Lu, Y, Sc) compounds at the temperature ranges (a) 450−600 °C and (b) 1000−1300 °C and graph of the dependence of the phase transition and melting temperatures vs radius of the rare earth cation.

structure in the example of $NaSrY(BO_3)_2$ compound. According to Rietveld refinement the low-temperature β-$NaSrY(BO_3)_2$ is isotypic to $KSrY(BO_3)_2$ crystallizing with a $P2_1/m$ space group (Figure 4). It should be noted that $KSrY(BO_3)_2$ has ordering of K and Sr ions in the asymmetric part of the unit cell, while in $NaSrY(BO_3)_2$ the cation positions of Na and Sr are disordered. There are two sites with different Na/Sr occupancies. The first site Na1/Sr1 has a ratio of 0.48(2)/0.52(2) and Na2/Sr2 has a ratio of 0.58(2)/0.42(2). The chemical formula can be written as $Sr_{0.94(2)}Na_{1.06(2)}Y(BO_3)_2$. The structure is composed from flat anionic BO_3 groups forming corrugated layers located parallel to the [010]. $[YO_6]$ octahedra are combined in packages and located between the layers. Na^+ and Sr^{2+} cations are located in the interpacket gap near the borate layers and are shifted to one of them.

The quality of XRD data on high-temperature $NaSrR(BO_3)_2$ was not enough for Rietveld refinement. So the structure was

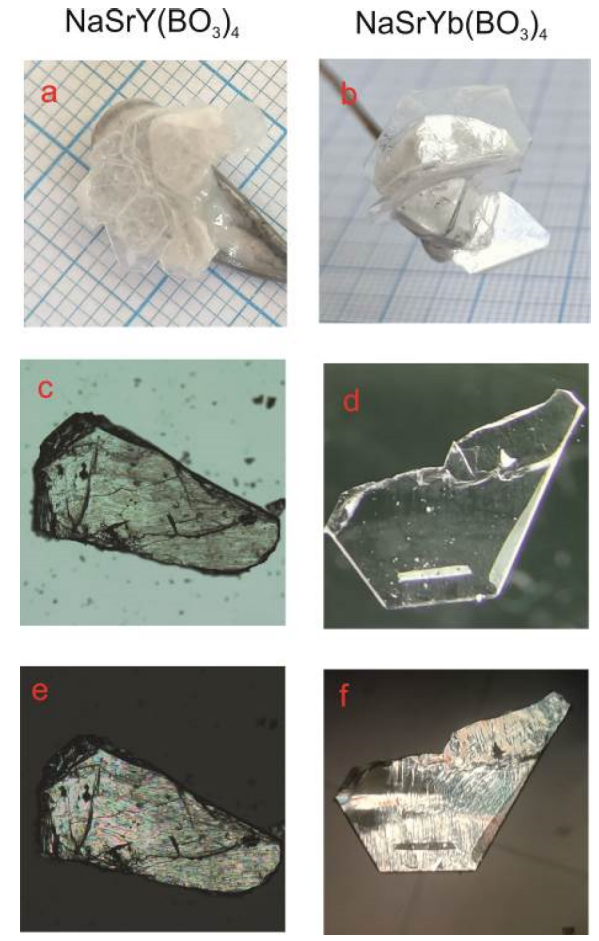

Figure 2. $NaSrR(BO_3)_2$ (R = Y, Yb) crystals: as grown druze (a,b) and selected samples under unpolarized (c,d) and polarized light (e,f).

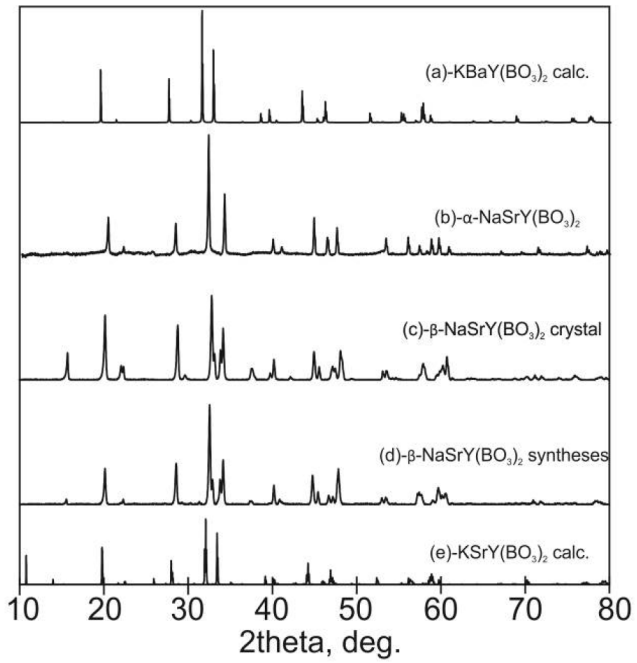

Figure 3. Measured XRD patterns of synthesized and grown $NaSrY(BO_3)_2$ crystals and calculated for $KSrY(BO_3)_2$ and $KBaR(BO_3)_2$.

https://doi.org/10.1021/acs.inorgchem.2c00596
Inorg. Chem. 2022, 61, 7497−7505

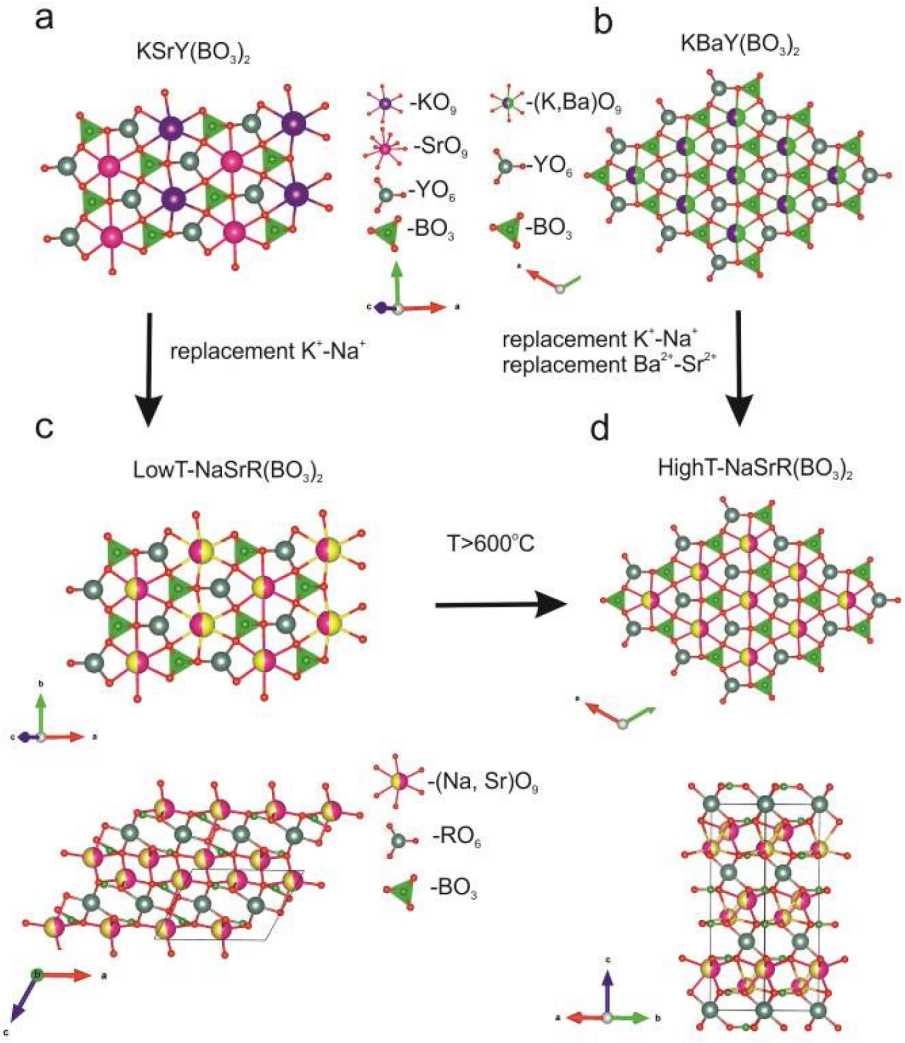

Figure 4. Structures projections of (a) $KBaY(BO_3)_2$,[19] (b) $KSrY(BO_3)_2$,[47] (c) β- $NaSrR(BO_3)_2$, and (d) α- $NaSrR(BO_3)_2$.

optimized within the density functional theory (DFT) implemented in the VASP package. First the algorithm was successfully verified on β-$NaSrY(BO_3)_2$. For high-temperature modification $KBaY(BO_3)_2$ as an initial model with replacement K-Ba to Na-Sr used. According to calculations, the high-temperature α-$NaSrR(BO_3)_2$ (R = Ho−Lu, Y, Sc) crystallizes with the $R\bar{3}m$ space group and are isotypic to $KBaY(BO_3)_2$ (Figure 4b). The structure can be described as layered, consisting of two layers of $[BO_3]^{3-}$ triangles. The oxygen atoms of these BO_3 triangles are distributed in space in such a way that octahedral voids are obtained, in the centers of which the REE are placed. In turn, such layers are interconnected by two sublayers formed by the disordered position of Na^+ and Sr^{2+} atoms (Figure 4d).

Theory group investigation of phase transition $R\bar{3}m \leftrightarrow P2_1/m$ using the ISODISTORT program[48] revealed that the transformation can be described by the emergence of instability at the (0, 1/2, 1) k_5-point (F) of the Brillouin zone of the high-symmetry R-3m unit cell (hereinafter the designation of irreducible representations (irrep) and points of the Brillouin zone are given in accordance with reference books.[49−51] The F^{2-} irrep drives this phase transition, and the transformation can be written as $R\bar{3}m \overset{F_2^-(\eta)}{\longleftrightarrow} P2_1/m$, where η is the critical order parameter. The analysis presents that this irrep allows a continuous phase transition. Cell parameters of the monoclinic unit cell can be obtained from the parent phase unit cell by using matrix: (1, −1, 0); (1, 1, 0); (−1/3, 1/3, 1/3) with shift of origin (1/3, 1/6, 1/6). It should be noted that the phase transition leads to charge ordering, asymmetric cell volume doubling, and splitting of positions. For example, one Sr/Na site in the R-3m phase splits into two sites for the $P2_1/m$ phase. The B site in R-3m splits into two sites also, but the O site splits into four sites in $P2_1/m$, and the Y site does not split at all.

Since low-temperature and high-temperature phases of $NaSrY(BO_3)_2$ contain the sites partially occupied by Sr and Na, we have constructed the ordered structural models of $NaSrY(BO_3)_2$ to perform the DFT calculations. In this case, the symmetry groups change: $P2_1/c \rightarrow P2_1/m$ (for low-temperature phase), $R\bar{3}m \rightarrow R3c$ (for high-temperature phase).

The local DFT optimization of $P2_1/m$ and $R3c$ models show that they retain their initial symmetry and atomic disposition. Optimized unit cell parameters correctly reproduce experimental ones (Table S5). The performed MD simulations show that atomic vibrations do not destroy crystal structures of $NaSrY(BO_3)_2$-$P2_1/m$ at 300 K and $NaSrY(BO_3)_2$-$R3c$ at 900 K. During the MD simulations, all BO_3 triangles preserve their geometry (angles and bond lengths), although sufficient

https://doi.org/10.1021/acs.inorgchem.2c00596
Inorg. Chem. 2022, 61, 7497−7505

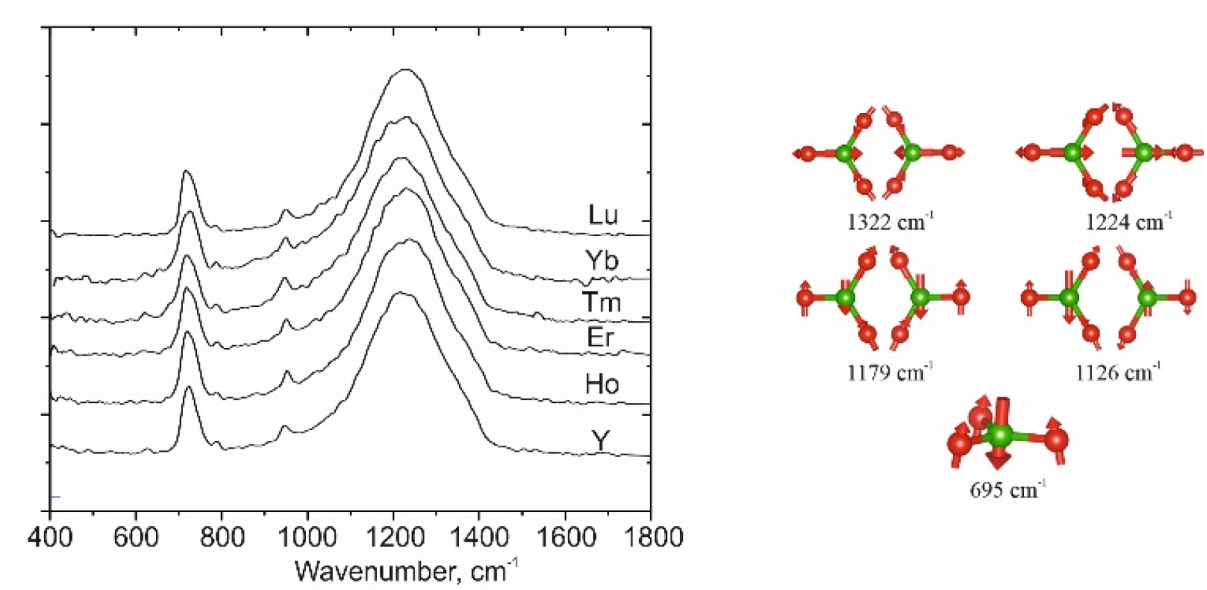

Figure 5. IR spectra for synthesized $NaSrR(BO_3)_2$ crystals and corresponding atomic shifts of BO_3 groups.

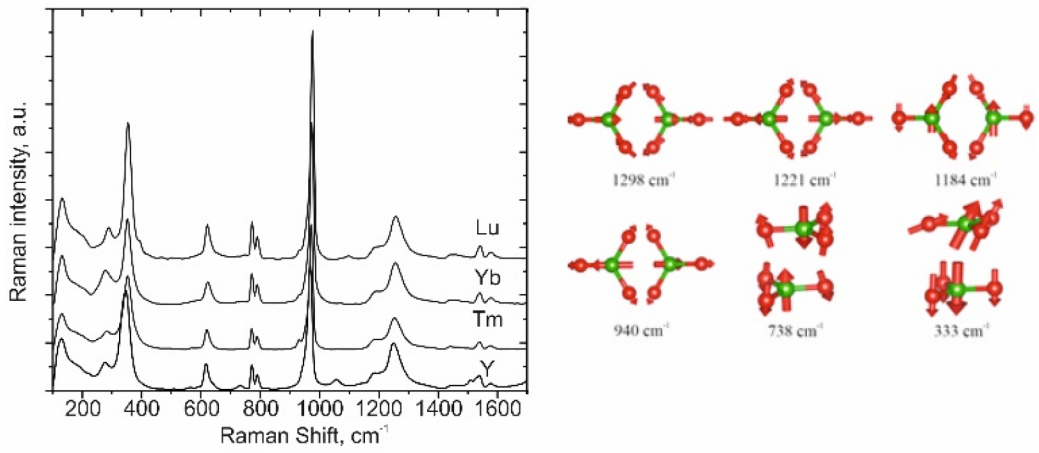

Figure 6. Raman spectra for synthesized $NaSrR(BO_3)_2$ crystals and corresponding atomic shifts of BO_3 groups.

wiggles of $[BO_3]^{-3}$ groups were observed (Figure S4 and Figure S5).

The calculated Raman and IR spectra are in good agreement with experimental ones (Figures S6 and S7). The atomic shifts at vibrations corresponding to the most intense IR and Raman peaks are shown in Figures 5 and 6. The active modes v_2 and v_4 in IR; v_2, v_3, and v_4 in Raman; v_1, v_2, v_3, and v_4 both in IR and Raman related to these polyhedra. Figure 5 shows IR spectra of $NaSrR(BO_3)_2$ crystals. BO_3 groups vibrations have two main modes v4 (stretching): 1208 1379 cm^{-1} and v2 (bending): 734, 782 cm^{-1}. Figure 6 shows Raman spectra with strong bands corresponding to BO_3 asymmetric stretching, stretching, out-of-plane bending, and bending vibration at 1335, 1525, 937, 710, 786, and 628 cm^{-1}, respectively. The NaO, SrO_6, and RO_9 octahedra vibration bands are likely to be located in the range 124−300 cm^{-1}.

Absorption spectra of $NaSrR(BO_3)_2$ (Ho−Lu, Y) in the range from 190 to 900 nm are shown in Figure 7a. The spectra for compounds with Yb, Lu, and Y do not have any peaks, while compounds containing Ho, Er, and Tm show typical absorption bands corresponding to transitions from the lower sublevel to the excited state of rare earth cations.

The photoluminescent emission spectra of the crystals are shown in Figure 7b. The spectrum of the $NaSrHo(BO_3)_2$ exhibits characteristic emissions attributed to the transitions in Ho^{3+} ions: luminescence lines in the 500−800 nm range due to emission $Ho^{3+5}I_8 \rightarrow {}^5S_2$, ${}^5F_5$, and ${}^5I_4$ transitions (~550, 664, and 754 nm). The main luminescence band of Er^{3+} lies in the IR region of the spectrum ~1550 nm (${}^4I_{13/2} \rightarrow {}^4I_{15/2}$). In addition to one, there are a number of shorter-wave bands of lower intensity related to the well-known electron transition ${}^4S_{3/2} \rightarrow {}^4I_{15/2}$ at 550 nm, ${}^4F_{9/2} \rightarrow {}^4I_{15/2}$ at 656 nm, ${}^4I_{9/2} \rightarrow {}^4I_{15/2}$ at 854 nm, and ${}^4I_{11/2} \rightarrow {}^4I_{15/2}$ at 956 nm. The sample with ytterbium has a characteristic emission band in the range of 950−1050 nm, related to the ${}^2F_{5/2} \rightarrow {}^2F_{7/2}$ transition.

Results of the total and partial DOS calculations of $NaSrY(BO_3)_2$-$P2_1/m$ are presented in Figure 8. The main portion of the valence band is broad, reaches ~6 eV, and is mainly due to contributions of O 2p states. The bottom of the conduction band is mainly composed of unoccupied 4d states

https://doi.org/10.1021/acs.inorgchem.2c00596
Inorg. Chem. 2022, 61, 7497−7505

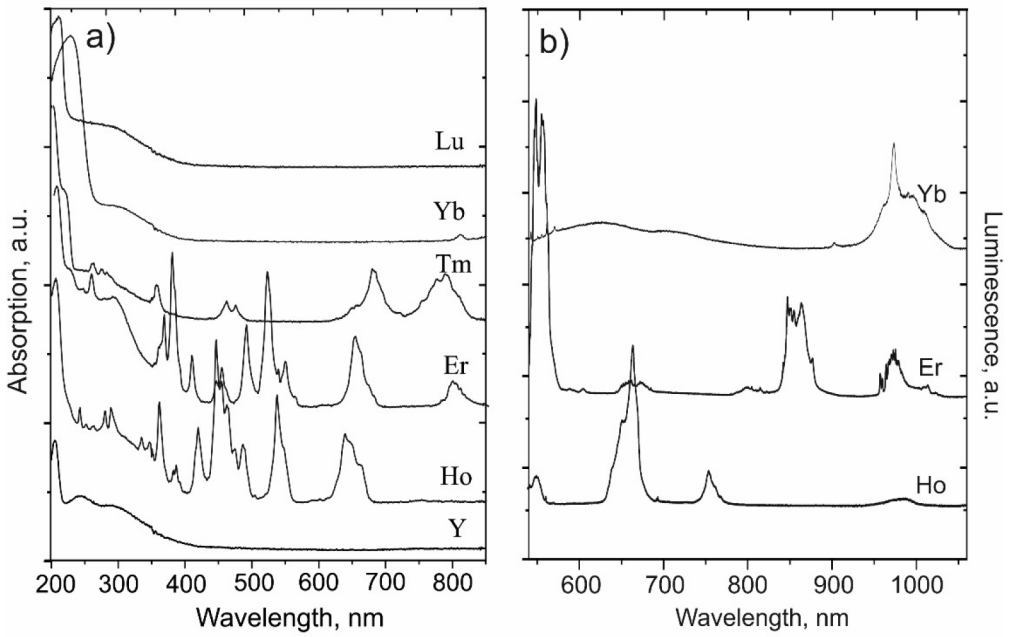

Figure 7. Absorption (a) and luminescence (b) spectra of $NaSrR(BO_3)_2$ (Ho−Lu, Y).

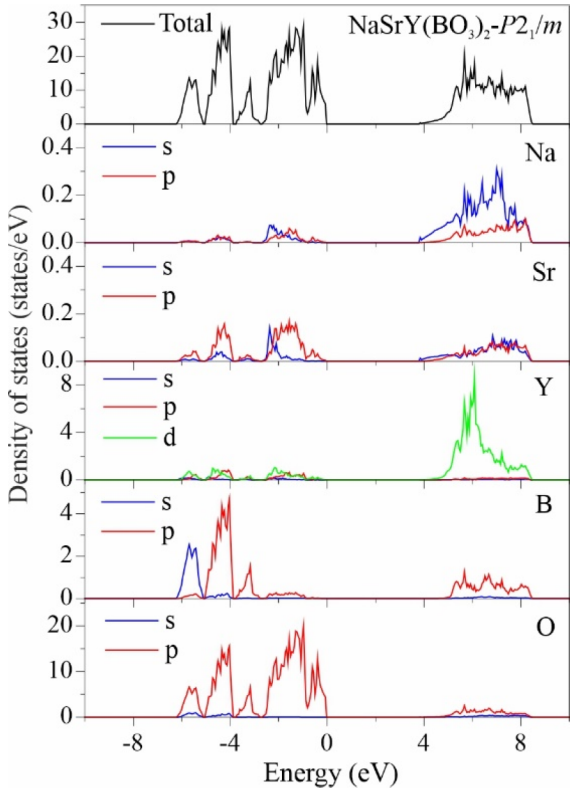

Figure 8. Total and partial DOS of $NaYSr(BO_3)_2$-$P2_1/m$.

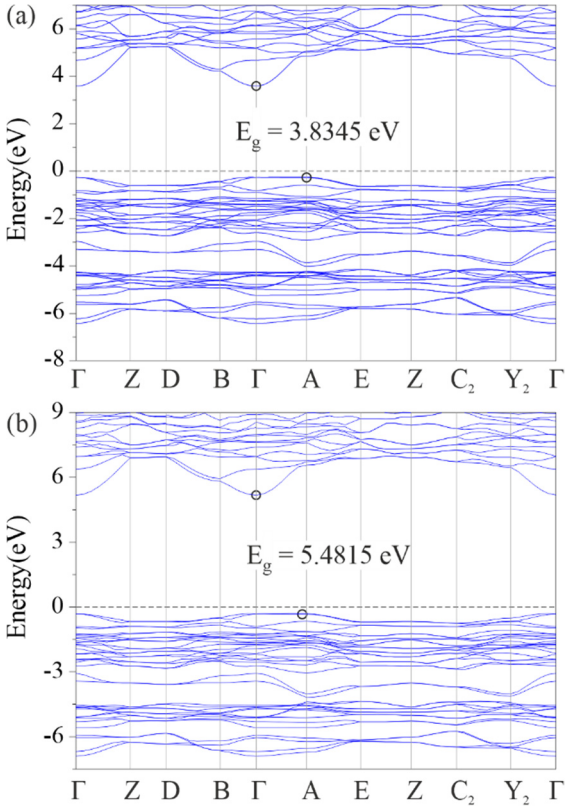

Figure 9. Calculated band structure of $NaSrY(BO_3)_2$-$P2_1/m$ with PBE (a) and HSE06 (b) functionals. The conduction band minimum and valence band maximum are denoted by open circles. The Fermi level is set at 0 eV.

of Y. The main contributors of upper bands in the conduction band region are unoccupied Y 3d, B 2p, and O 2p.

According to our PBE calculations, $NaSrY(BO_3)_2$-$P2_1/m$ is dielectric with an indirect band gap of 3.8345 eV along the Γ−*A* direction (Figure 9a). It should be noted that the direct band gap in the Γ-point is equal to 3.8438 eV. This difference is small to make a conclusion about the nature of the band gap in $NaSrY(BO_3)_2$-$P2_1/m$. Since the use of the PBE functional usually tends to underestimate the width of band gap, the HSE06 hybrid functional was also used to calculate band structures of $NaSrY(BO_3)_2$-$P2_1/m$. Both methods resulted in qualitatively the same band structure. The width of the band gap obtained using HSE06 is equal to 5.4815 eV (Figure 9b)

https://doi.org/10.1021/acs.inorgchem.2c00596
Inorg. Chem. 2022, 61, 7497−7505

and coincides well with the experimentally obtained value (~5.85 eV).

Theoretical estimation of the band gap by DFT calculations is consistent with experimental spectra. For example, the $NaYSr(BO_3)_2$ sample (where the yttrium ion has no pronounced absorption bands in contrast to Tm, Er, Ho) has the "shoulder" at 350−400 nm at the long-wavelength region of the spectrum and the absorption edge of the intense short-wavelength band in the 200−210 nm region (Figure 7). Experimental estimation of the band gap by the Tauc method for the long-wave band (assuming an indirect transition) and for the short-wave band (assuming a direct transition) gave the values ~3.2 eV and ~5.85 eV, respectively. The results obtained by the DASF method showed ~3.5 eV and ~5.85 eV, respectively. The data for the $NaLuSr(BO_3)_2$ sample are the following: ~3.0 eV and ~5.55 eV by the Tauc method and 3.2 and 5.64 eV by the DASF method, respectively.

CONCLUSIONS

$NaSrR(BO_3)_2$ (R = Ho−Lu, Y, Sc) compounds were obtained by the solid-state synthesis and flux crystal growth. According to Rietveld refinement and theoretical calculations, these crystals belong to $P2_1/m$ (low temperature) and $R\bar{3}m$ (high temperature modification) space groups. Based on DSC results, phase transition and melting temperatures of these compounds were found. The diffuse optical reflectance and luminescent properties of powdered $NaSrR(BO_3)_2$ (Ho−Lu, Y) were studied. The obtained compounds might be considered as effective IR phosphores or matrixes for creating hidden, machine-readable fluorescent labels used to protect securities as well as an active medium for lasers that generate in a spectral range safe for the human eye (1.5−1.6 μm).

ASSOCIATED CONTENT

Supporting Information

The Supporting Information is available free of charge at https://pubs.acs.org/doi/10.1021/acs.inorgchem.2c00596.

Figure S1, XRD pattern of the synthesized $NaSrR(BO_3)_2$ (R = Ho−Lu, Y, Sc) recorded at room temperature; Figure S2, XRD pattern of synthesized $NaSrR(BO_3)_2$ (R = Ho, Er, Yb, and Y) recorded in situ at 600 °C; Figure S3, difference Rietveld plot of $NaSrY(BO_3)_2$; Figure S4, initial static structure of $NaSrY(BO_3)_2$-$P2_1/m$ and the last snapshot of the structure after 1 ps at 300 K based on the molecular dynamic simulation; Figure S5, initial static structure of $NaSrY(BO_3)_2$-$R3c$ and the last snapshot of the structure after 1 ps at 900 K based on the molecular dynamic simulation; Figure S6, calculated IR spectra of $NaSrY(BO_3)_2$-$P2_1/m$; Figure S7, calculated Raman spectra of $NaSrY(BO_3)_2$-$P2_1/m$; Table S1, technical details of powder X-ray analyses $NaSrY(BO_3)_2$; Table S2, final atomic coordinates, equivalent isotropic displacement parameters of $NaSrY(BO_3)_2$; Table S3, unit cell parameters of low temperature $NaSrR(BO_3)_2$, (R = Ho−Lu, Y, Sc), calculated with XRD data; Table S4, unit cell parameters of high temperature $NaSrR(BO_3)_2$, (R = Ho, Er, Yb, and Y) calculated with XRD data; and Table S5, optimized unit cell parameters of $NaSrY(BO_3)_2$-$P2_1/m$ and $NaSrY(BO_3)_2R$-3c compared with experimental data (PDF)

Accession Codes

CCDC 2153789 contains the supplementary crystallographic data for this paper. These data can be obtained free of charge via www.ccdc.cam.ac.uk/data_request/cif, or by emailing data_request@ccdc.cam.ac.uk, or by contacting The Cambridge Crystallographic Data Centre, 12 Union Road, Cambridge CB2 1EZ, UK; fax: +44 1223 336033.

AUTHOR INFORMATION

Corresponding Author

Artem B. Kuznetsov − *Sobolev Institute of Geology and Mineralogy SB RAS, Novosibirsk 630090, Russia;* orcid.org/0000-0003-3808-8098; Email: ku.artemy@igm.nsc.ru

Authors

Konstantin A. Kokh − *Sobolev Institute of Geology and Mineralogy SB RAS, Novosibirsk 630090, Russia; Novosibirsk State University, Novosibirsk 630090, Russia; Kemerovo State University, Kemerovo 650000, Russia;* orcid.org/0000-0003-1967-9642

Nursultan Sagatov − *Sobolev Institute of Geology and Mineralogy SB RAS, Novosibirsk 630090, Russia;* orcid.org/0000-0001-5158-3523

Pavel N. Gavryushkin − *Sobolev Institute of Geology and Mineralogy SB RAS, Novosibirsk 630090, Russia; Novosibirsk State University, Novosibirsk 630090, Russia*

Maksim S. Molokeev − *Kemerovo State University, Kemerovo 650000, Russia; Kirensky Institute of Physics, Siberian Branch, Russian Academy of Sciences, Krasnoyarsk 660036, Russian Federation;* orcid.org/0000-0002-8297-0945

Valery A. Svetlichnyi − *Tomsk State University, Tomsk 634050, Russia;* orcid.org/0000-0002-3935-0871

Ivan N. Lapin − *Tomsk State University, Tomsk 634050, Russia;* orcid.org/0000-0001-5736-3791

Nadezda G. Kononova − *Sobolev Institute of Geology and Mineralogy SB RAS, Novosibirsk 630090, Russia*

Vyacheslav S. Shevchenko − *Sobolev Institute of Geology and Mineralogy SB RAS, Novosibirsk 630090, Russia*

Asset Bolatov − *Al-Farabi Kazakh National University, Center of Physical-Chemical Methods of Research and Analysis, Almaty 050040, Kazakhstan*

Bolat Uralbekov − *Al-Farabi Kazakh National University, Center of Physical-Chemical Methods of Research and Analysis, Almaty 050040, Kazakhstan*

Anastasia A. Goreiavcheva − *Sobolev Institute of Geology and Mineralogy SB RAS, Novosibirsk 630090, Russia*

Alexander E. Kokh − *Sobolev Institute of Geology and Mineralogy SB RAS, Novosibirsk 630090, Russia*

Complete contact information is available at: https://pubs.acs.org/10.1021/acs.inorgchem.2c00596

Author Contributions

Artem B. Kuznetsov, writing of the original draft; Konstantin A. Kokh, Vyacheslav S. Shevchenko, and Pavel N. Gavryushkin, writing, review, and editing; Nursultan Sagatov, Maksim S. Molokeev, Valery A. Svetlichnyi, and Ivan N. Lapin, investigation; Anastasia A. Goreiavcheva, Nadezda G. Kononova, and Asset Bolatov, methodology; Bolat Uralbekov, supervision; Alexander E. Kokh, project administration.

Funding

This work was supported by Grant GF MES RK "Crystallochemical design of the new alkali and rare earth-

https://doi.org/10.1021/acs.inorgchem.2c00596
Inorg. Chem. 2022, 61, 7497−7505

based borate phosphors", Grant IRN AP08855427, and the state assigned project of IGM SB RAS.

Notes

The authors declare no competing financial interest.

REFERENCES

(1) Kushida, T. Energy Transfer and Cooperative Optical Transitions in Rare-Earth Doped Inorganic Materials. III. Dominant Transfer Mechanism. *J. Phys. Soc. Jpn.* **1973**, *34* (5), 1334−1337.
(2) Reisfeld, R.; Saraidarov, T.; Ziganski, E.; Gaft, M.; Lis, S.; Pietraszkiewicz, M. Intensification of rare earths luminescence in glasses. *J. Lumin.* **2003**, *102*−*103*, 243−247.
(3) Ryba-Romanowski, W.; Solarz, P.; Dominiak-Dzik, G.; Gusowski, M. New luminescent systems based on fluoride crystals doped with rare earth ions. *Opt. Mater.* **2006**, *28* (1), 77−84.
(4) Smentek, L.; Andes Hess, B. Theory of host sensitized luminescence of rare earth doped materials. I. Parity considerations. *J. Alloys Compd.* **2000**, *300*−*301*, 165−173.
(5) Verma, S.; Verma, K.; Kumar, D.; Chaudhary, B.; Som, S.; Sharma, V.; Kumar, V.; Swart, H. C. Recent advances in rare earth doped alkali-alkaline earth borates for solid state lighting applications. *Physica B: Condensed Matter* **2018**, *535*, 106−113.
(6) Uralbekov, B.; Shevchenko, V.; Kuznetsov, A.; Kokh, A.; Kononova, N.; Bolatov, A.; Kokh, K. Novel compounds in the MMeR(BO3)2 borate family (M = alkali metal, Me= alkaline earth metal, R= rare-earth element): Syntheses, crystal structures and luminescent properties. *J. Lumin.* **2019**, *216*, 116712.
(7) Chen, P.; Murshed, M. M.; Fischer, M.; Frederichs, T.; Gesing, T. M. KLi2RE(BO3)2 (RE = Dy, Ho, Er, Tm, Yb, and Y): Structural, Spectroscopic, And Thermogravimetric Studies on a Series of Mixed-Alkali Rare-Earth Orthoborates. *Inorg. Chem.* **2020**, *59*, 18214.
(8) Chen, P.; Murshed, M. M.; Gesing, T. M. Synthesis and crystal structures of novel alkali rare-earth orthoborates K3RE3(BO3)4 (RE = Pr, Nd, Sm−Lu). *J. Mater. Sci.* **2021**, *56* (5), 3639−3652.
(9) Rambabu, U.; Annapurna, K.; Balaji, T.; Satyanarayana, J. V.; Rajamohan Reddy, K.; Buddhudu, S. Fluorescence Spectra of Eu3+ and Tb3+ Doped Na6 Ln (BO3)3 (Ln = La, Gd, Y) Phosphors. *Spectrosc. Lett.* **1996**, *29* (5), 833−839.
(10) Shablinskii, A. P.; Bubnova, R. S.; Kolesnikov, I. E.; Krzhizhanovskaya, M. G.; Povolotskiy, A. V.; Ugolkov, V. L.; Filatov, S. K. Novel Sr3Bi2(BO3)4:Eu3+ red phosphor: Synthesis, crystal structure, luminescent and thermal properties. *Solid State Sci.* **2017**, *70*, 93−100.
(11) Zhang, Y.; Li, Y. Red photoluminescence and crystal structure of Sr3Y2(BO3)4. *J. Alloys Compd.* **2004**, *384* (1), 88−92.
(12) Seryotkin, Y. V.; Bakakin, V. V.; Kokh, A. E.; Kononova, N. G.; Svetlyakova, T. N.; Kokh, K. A.; Drebushchak, T. N. Synthesis and crystal structure of new layered BaNaSc(BO3)2 and BaNaY(BO3)2 orthoborates. *J. Solid State Chem.* **2010**, *183* (5), 1200−1204.
(13) Svetlyakova, T. N.; Kokh, A. E.; Kononova, N. G.; Fedorov, P. P.; Rashchenko, S. V.; Maillard, A. Search for compounds of the NaBaR(BO3)2 family (R = La, Nd, Gd, and Yb) and the new NaBaYb(BO3)2 orthoborate. *Crystallography Reports* **2013**, *58* (1), 54−60.
(14) Geng, W.; Zhou, X.; Ding, J.; Wang, Y. NaBaY(BO3)2:Ce3+, Tb3+: A novel sharp green-emitting phosphor used for WLED and FEDs. *J. Am. Ceram. Soc.* **2018**, *101* (10), 4560−4571.
(15) Tang, H.; Li, Y.; Yang, R.; Gao, W. Phase formations and red-luminescence enhancement of Eu3+-activated NaBaY(BO3)2 phosphors. *J. Lumin.* **2019**, *208*, 253−258.
(16) Qiao, X.; Xin, J.; Nie, X.; Xu, J.; Qi, S.; Jiang, Z. The structure-dependent luminescence of Eu3+-activated MBaY(BO3)2 (M = Na, K) nanoparticles. *Dyes Pigm.* **2017**, *143*, 103−111.
(17) Geng, W.; Zhou, X.; Ding, J.; Wang, Y. Density-functional theory calculations, luminescence properties and fluorescence ratiometric thermo-sensitivity for a novel borate based red phosphor: NaBaSc(BO3)2:Ce3+, Mn2+. *Journal of Materials Chemistry C* **2019**, *7* (7), 1982−1990.
(18) Shevchenko, V. S.; Kononova, N. G.; Kokh, A. E.; Bolatov, A. K.; Uralbekov, B. M.; Burkitbaev, M. M. KBaR(BO3)2 orthoborates (R = REE): Synthesis and study. *Russ. J. Inorg. Chem.* **2017**, *62* (9), 1177−1181.
(19) Gao, J.; Song, L.; Hu, X.; Zhang, D. A buetschliite-type rare-earth borate, KBaY(BO3)2. *Solid State Sci.* **2011**, *13* (1), 115−119.
(20) Kuznetsov, A. B.; Kokh, K. A.; Kononova, N. G.; Shevchenko, V. S.; Kaneva, E. V.; Uralbekov, B.; Svetlichnyi, V. A.; Kokh, A. E. Synthesis and growth of new rare earth borates KCaR(BO3)2 (R= La, Pr and Nd). *J. Solid State Chem.* **2020**, *282*, 121091.
(21) Kuznetsov, A. B.; Kokh, K. A.; Kononova, N. G.; Shevchenko, V. S.; Rashchenko, S. V.; Uralbekov, B.; Svetlichnyi, V. A.; Simonova, E. A.; Kokh, A. E. Growth and crystal structure of Li3Ba4Sc3B8O22 borate and its Tb3+ doped green-emitting phosphor. *J. Lumin.* **2020**, *217*, 116755.
(22) Chen, P.; Xia, M.; Li, R. K. A terbium rich orthoborate LiSrTb2(BO3)3 and its analogues. *New J. Chem.* **2015**, *39* (12), 9389−9395.
(23) Kokh, A. E.; Kononova, N. G.; Shevchenko, V. S.; Seryotkin, Y. V.; Bolatov, A. K.; Abdullin, K. A.; Uralbekov, B. M.; Burkitbayev, M. Syntheses, crystal structure and luminescence properties of the novel isostructural KSrR(BO 3) 2 with R = Y, Yb, Tb. *J. Alloys Compd.* **2017**, *711*, 440−445.
(24) Zeng, Q. D.; Li, R. K. A new type of orthoborates: ASr4La3(BO3)6 (A = Li, Na). *Solid State Sci.* **2014**, *29*, 75−78.
(25) Mutailipu, M.; Xie, Z.; Su, X.; Zhang, M.; Wang, Y.; Yang, Z.; Janjua, M. R. S. A.; Pan, S. Chemical Cosubstitution-Oriented Design of Rare-Earth Borates as Potential Ultraviolet Nonlinear Optical Materials. *J. Am. Chem. Soc.* **2017**, *139* (50), 18397−18405.
(26) Kuznetsov, A. B.; Ezhov, D. M.; Kokh, K. A.; Kononova, N. G.; Shevchenko, V. S.; Rashchenko, S. V.; Pestryakov, E. V.; Svetlichnyi, V. A.; Lapin, I. N.; Kokh, A. E. Flux growth and optical properties of K7CaY2(B5O10)3 nonlinear crystal. *Mater. Res. Bull.* **2018**, *107*, 333−338.
(27) Kuznetsov, A. B.; Ezhov, D. M.; Kokh, K. A.; Kononova, N. G.; Shevchenko, V. S.; Uralbekov, B.; Bolatov, A.; Svetlichnyi, V. A.; Lapin, I. N.; Simonova, E. A.; Kokh, A. E. Nonlinear optical crystals K7CaR2(B5O10)3 (R = Nd, Yb), growth and properties. *J. Cryst. Growth* **2019**, *519*, 54−59.
(28) Chen, X.; Bian, R.; Chang, X.; Xiao, W. A new rare-earth borate Na3−3δEu2+δ(BO3)3 (δ = 0.16): Synthesis, crystal structure, vibrational spectra, and luminescent properties. *Solid State Sci.* **2021**, *113*, 106540.
(29) Ullah, I.; Khan, I.; Shah, S. K.; Khattak, S. A.; Shoaib, M.; Kaewkhao, J.; Ahmad, T.; Ahmed, E.; Rooh, G.; Khan, A. Luminescence properties of Sm3+ doped Na2B4O7 glasses for lighting application. *J. Lumin.* **2021**, *230*, 117700.
(30) Zhao, D.; Li, Y.-N.; Fan, Y.-P.; Liu, B.-Z.; Zhang, S.-R.; Zhang, R.-J. Crystal structure, theoretical studies and luminescent properties of a new borate Na3GdB8O15 with one-dimensional broad-banded anionic framework. *Dalton Transactions* **2020**, *49* (37), 13167−13175.
(31) Mascetti, J.; Fouassier, C.; Hagenmuller, P. Concentration quenching of the Nd3+ emission in alkali rare earth borates. *J. Solid State Chem.* **1983**, *50* (2), 204−212.
(32) Li, Z.; Zeng, J.; Zhang, G.; Li, Y. A new promising phosphor, Na3La2(BO3)3:Ln (Ln = Eu, Tb). *J. Solid State Chem.* **2005**, *178* (12), 3624−3630.
(33) Qiao, X.; Seo, H. J. Phase transition, structural and spectroscopic properties of Ba3Y(BO3)3 phosphor. *J. Alloys Compd.* **2015**, *637*, 504−508.
(34) Shan, F.; Kang, L.; Zhang, G.; Yao, J.; Lin, Z.; Xia, M.; Zhang, X.; Fu, Y.; Wu, Y. Na3Y3(BO3)4: a new noncentrosymmetric borate with an open-framework structure. *Dalton Transactions* **2016**, *45* (17), 7205−7208.
(35) *Bruker AXS TOPAS V4: General profile and structure analysis software for powder diffraction data, User's Manual*; Bruker AXS: Karlsruhe, Germany, 2008.

https://doi.org/10.1021/acs.inorgchem.2c00596
Inorg. Chem. 2022, 61, 7497−7505

(36) *The Rietveld Method*, Young, R. A., Ed.; IUCr Monographs in Crystallography, *5*, Oxford University Press: Oxford, U.K., 1993; pp 252−254.
(37) Toby, B. H.; Von Dreele, R. B. GSAS-II: the genesis of a modern open-source all purpose crystallography software package. *J. Appl. Crystallogr.* **2013**, *46* (2), 544−549.
(38) Dolgonos, A.; Mason, T. O.; Poeppelmeier, K. R. Direct optical band gap measurement in polycrystalline semiconductors: A critical look at the Tauc method. *J. Solid State Chem.* **2016**, *240*, 43−48.
(39) Souri, D.; Tahan, Z. E. A new method for the determination of optical band gap and the nature of optical transitions in semiconductors. *Appl. Phys. B: Laser Opt.* **2015**, *119* (2), 273−279.
(40) Kresse, G.; Furthmüller, J. Efficient iterative schemes for ab initio total-energy calculations using a plane-wave basis set. *Phys. Rev. B* **1996**, *54* (16), 11169−11186.
(41) Kresse, G.; Joubert, D. From ultrasoft pseudopotentials to the projector augmented-wave method. *Phys. Rev. B* **1999**, *59* (3), 1758−1775.
(42) Perdew, J. P.; Burke, K.; Ernzerhof, M. Generalized Gradient Approximation Made Simple. *Phys. Rev. Lett.* **1996**, *77* (18), 3865−3868.
(43) Wang, J.; You, J.; Wang, M.; Lu, L.; Wan, S.; Sobol, A. A. In-situ studies on the micro-structure evolution of A2W2O7 (A = Li, Na, K) during melting by high temperature Raman spectroscopy and density functional theory. *Spectrochimica Acta Part A: Molecular and Biomolecular Spectroscopy* **2017**, *185*, 188−196.
(44) Ma, N.; You, J.; Lu, L.; Wang, J.; Wang, M.; Wan, S. Microstructure studies of the molten binary K3AlF6−Al2O3 system by in situ high temperature Raman spectroscopy and theoretical simulation. *Inorganic Chemistry Frontiers* **2018**, *5* (8), 1861−1868.
(45) Zhang, S.; Wan, S.; Zeng, Y.; Jiang, S.; Gong, X.; You, J. In Situ Raman Spectroscopy and DFT Studies of the Li2GeO3Melt Structure. *Inorg. Chem.* **2019**, *58* (8), 5025−5030.
(46) Fonari, A.; Stauffer, S. *vasp_raman.py*, 2013; https://github.com/raman-sc/VASP/.
(47) Kokh, A. E.; Kononova, N. G.; Shevchenko, V. S.; Seryotkin, Y. V.; Bolatov, A. K.; Abdullin, K. A.; Uralbekov, B. M.; Burkitbayev, M. Syntheses, crystal structure and luminescence properties of the novel isostructural KSrR(BO3)2 with R = Y, Yb, Tb. *J. Alloys Compd.* **2017**, *711*, 440−445.
(48) Campbell, B. J.; Stokes, H. T.; Tanner, D. E.; Hatch, D. M. ISODISPLACE: a web-based tool for exploring structural distortions. *J. Appl. Crystallogr.* **2006**, *39* (4), 607−614.
(49) Kovalev, O. V.; Stokes, H. T.; Hatch, D. M. *Representations of the Crystallographic Space Groups: Irreducible Representations, Induced Representations, And Corepresentations*; Gordon and Breach: Yverdon, Switzerland; Langhorne, PA, 1993.
(50) Kovalev, O. V. *Representations of the Crystallographic Space Groups: Irreducible Representations, Induced Representations, and Corepresentations*; Gordon and Breach: Yverdon, Switzerland; Langhorne, PA, 1993.
(51) Miller, S. C.; Love, W. F. *Tables of Irreducible Representations of Space Groups and Co-Representations of Magnetic Space Groups*; Pruett Press, 1967.

Recommended by ACS

Noncentrosymmetric Rb3(COOH)3(H3BO3)2 vs Centrosymmetric Cs3(COOH)3(H3BO3)2
Yunqiao Guo, Guohong Zou, *et al.*
SEPTEMBER 17, 2021
CRYSTAL GROWTH & DESIGN
READ

Phosphorescence in Mn4+-Doped R+/R2+ Germanates (R+ = Na+ or K+, R2+ = Sr2+)
Sergei A. Novikov, Yurij Mozharivskyj, *et al.*
JUNE 08, 2022
INORGANIC CHEMISTRY
READ

La2SrB10O19: A Promising Ultraviolet Nonlinear Optical Crystal with an Enhanced Nonlinear Optical Effect and Shortened Cutoff Edge
Jingcheng Feng, Guochun Zhang, *et al.*
JULY 13, 2020
CRYSTAL GROWTH & DESIGN
READ

Struvite-type AMgPO4·6H2O (A = NH4, K): Two Natural Deep-Ultraviolet Transparent Nonlinear Optical Crystals
Feifei Yuan, Zhoubin Lin, *et al.*
MAY 24, 2021
INORGANIC CHEMISTRY
READ

Get More Suggestions >

https://doi.org/10.1021/acs.inorgchem.2c00596
Inorg. Chem. 2022, 61, 7497−7505